

## Reply to the comments and List of relevant changes

We thank the editor for these new comments. All the suggested changes have been incorporated in the revised version of the manuscript. Here it follows the list of the relevant changes.

- References have been listed in chronological order, as suggested, at lines 36, 46, 51, 94, 269, 272, 275, 290.
- A new reference about the Camaiore sinkhole has been included in the new version of the manuscript at line 91 and in figure 1. We referred to *Buchignani, V., D'Amato Avanzi, G., Giannecchini, R., Puccinelli, A.: Evaporite karst and sinkholes: a synthesis on the case of Camaiore (Italy). Environmental Geology, 53, 1037-1044. <https://doi.org/10.1007/s00254-007-0730-x>, 2008.*
- We better described the vegetation at Prà di Lama and its impact on the coherence loss at lines 191-193
- We provided further information about the book “Pieve Fosciana Ieri e Oggi” by adding the “Amministrazione Comunale di Pieve Fosciana” as editor. We also added the place and the number of pages.

1 GROWTH OF A SINKHOLE IN A SEISMIC ZONE OF THE NORTHERN APENNINES (ITALY)  
2 Alessandro La Rosa<sup>1,2</sup>, Carolina Pagli<sup>2</sup>, Giancarlo Molli<sup>2</sup>, Francesco Casu<sup>3</sup>, Claudio De Luca<sup>3</sup>, Amerino  
3 Pieroni<sup>4</sup> and Giacomo D'amato Avanzi<sup>2</sup>

4  
5 <sup>1</sup>Dipartimento di Scienze della Terra, Università degli Studi di Firenze, Via G. La Pira, 4, 50121 Firenze, Italy  
6 <sup>2</sup> Dipartimento di Scienze della Terra, Università di Pisa, Via S. Maria, 53, 56126 Pisa, Italy  
7 <sup>3</sup> CNR, Consiglio Nazionale delle Ricerche, Istituto per il Rilevamento Elettromagnetico dell'Ambiente (IREA-  
8 CNR), Via Diocleziano, 328, 80124 Napoli, Italy  
9 <sup>4</sup> Pro.Geo. s.r.l. Via Valmaira, 14, 55032, Castelnuovo di Garfagnana, Italy

10  
11 **Keywords:** Sinkhole, InSAR, Seismicity

12 **Abstract**

13 Sinkhole collapse is a major hazard causing substantial social and economic losses. However,  
14 the surface deformations and sinkhole evolution are rarely recorded, as these sites are known  
15 mainly after a collapse, making the assessment of sinkholes-related hazard challenging.  
16 Furthermore, more than 40% of the sinkholes of Italy are in seismically hazardous zones; it remains  
17 unclear whether seismicity may trigger sinkhole collapse. Here we use a multidisciplinary dataset of  
18 InSAR, surface mapping and historical records of sinkhole activity to show that the Prà di Lama lake  
19 is a long-lived sinkhole that was formed over a century ago in an active fault zone and grew through  
20 several events of unrest characterized by episodic subsidence and lake-level changes. Moreover,  
21 InSAR shows that continuous aseismic subsidence at rates of up to 7.1 mm yr<sup>-1</sup> occurred during  
22 2003-2008, between events of unrest. Earthquakes on the major faults near the sinkhole are not a  
23 trigger to sinkhole activity but small-magnitude earthquakes at 4-12 km depth occurred during  
24 sinkhole unrest in 1996 and 2016. We interpret our observations as evidence of seismic creep in an  
25 active fault zone at depth causing fracturing and ultimately leading to the formation and growth of  
26 the Prà di Lama sinkhole.

27

28        **1. Introduction**

29        Sinkholes are closed depressions with internal drainage typically associated with karst  
30        environments, where the exposed soluble rocks are dissolved by circulating ground water  
31        (dissolution sinkholes) but other types of sinkholes also exist. Subsidence sinkholes, for example,  
32        can form for both internal erosion and dissolution of covered layers leading to downward  
33        gravitational deformations such as collapse, sagging or suffosion (*Ford and Williams, 2007; Gutiérrez*  
34        *et al., 2008; Gutiérrez et al., 2014*). Deep sinkholes have been often observed along seismically active  
35        faults indicating a causal link between sinkhole formation and active tectonics (*Faccenna et al.,*  
36        *1993; Harrison et al., 2002; Closson et al., 2005; Florea, 2005; Harrison et al., 2002; Del Prete et al.,*  
37        *2010; Parise et al., 2010; Wadas et al., 2017*). In some cases, the processes responsible for the ~~ir~~  
38        formation ~~of these sinkholes~~ have been attributed to fracturing and increased permeability in the  
39        fault damage zone promoting fluid circulation and weathering of soluble rocks at depth.  
40        Additionally, when carbonate bedrocks lie below thick non-carbonate formations, stress changes  
41        caused by faulting may cause decompression of confined aquifers favouring upward migration of  
42        deep fluids, hence promoting erosion and collapses (e.g. *Harrison et al., 2002; Wadas et al., 2017*).  
43        Seismically-induced stress changes could also trigger collapse of unstable cavities as in the case of  
44        the two sinkholes that formed near En Gedi (Dead Sea) following the  $M_w$  5.2 earthquake on the Dead  
45        Sea Transform Fault in 2004 (*Salamon, 2004*). Sinkhole subsidence and collapses are a major hazard  
46        and cause substantial economic and human losses globally (*Frumkin and Raz, 2001; Closson, 2005;*  
47        *Wadas, 2017; Closson, 2005*).

48        In Italy, a total of 750 sinkholes have been identified and the 40% of them are along active  
49        faults (*Caramanna et al., 2008*) but this number could be underestimated due to the high frequency  
50        of sinkholes both related to karst and anthropogenic origin (*Parise and Vennari, 2013*). Seismicity

51 induced sinkhole deformation have been often observed in Italy (e.g. [Santo et al., 2007](#); [Parise et al., 2010](#); [Kawashima et al., 2010](#); [Santo et al., 2007](#)).

53 The sinkhole of Prà di Lama, near the [village of](#) Pieve Fosciana ~~town~~ (Lucca [province](#), Italy), is  
54 a quasi-circular depression filled by a lake. Prà di Lama is located in the seismically active Apennine  
55 range of Northern Tuscany, at the intersection between two active faults (Fig. 1). Hot springs are  
56 also present at Pieve Fosciana suggesting that fluid migration along the faults planes occurs. Sudden  
57 lake-level changes of up to several meters, ground subsidence, surface fracturing and seismicity  
58 have occurred repeatedly since at least 991 A.D. ([Nisio, 2008](#)). The most recent deformation events  
59 occurred in March 1996 and between May 2016 and October 2017. However, the processes that  
60 control the growth of the Prà di Lama sinkhole remain unclear. Furthermore, whether seismicity  
61 along the active faults around Prà di Lama may trigger sinkhole subsidence or collapse is debated.

62 In this paper we combine recent InSAR observations, seismicity, and surface mapping, as well  
63 as historical records of lake-level changes and ground subsidence at the Prà di Lama from 1828 to  
64 understand the mechanisms of sinkhole growth in an active fault system.

65 **2. Geological setting**

66 The area of the Prà di Lama sinkhole is located within the Garfagnana basin (Fig.1), an  
67 extensional graben in the western Northern Apennines, a NW-SE trending fold-and-thrust belt  
68 formed by the stack of different tectonic units caused by the convergence of the Corsica-European  
69 and Adria plates. The current tectonic regime of the Apennines is characterized by shortening in the  
70 eastern sector of the Apennine range and extension in the westernmost side of the range ([Elter et al., 1975](#); [Patacca and Scandone, 1989](#); [Bennett et al., 2012](#)). The contemporaneous eastward  
71 migration of shortening and upper plate extension are believed to be caused by the roll-back  
72 subduction during the counter-clockwise rotation of the Adria plate ([Doglioni, 1991](#); [Meletti et al., 2000](#); [Serpelloni et al., 2005](#); [Faccenna et al., 2014](#); [Le Breton et al., 2017](#)). Extension started 4-5 Ma

75 ago leading to the formation of several NW-SE-oriented grabens, bounded by NE-dipping and SW-  
76 dipping normal faults that are dissected by several NE-trending, right-lateral strike-slip faults (Fig.  
77 1). The inner northern Apennines are a seismically active area, where several earthquakes with  $M_w$   
78 > 5 occurred, including the largest instrumentally recorded earthquake,  $M_w$  6.5, in 1920 (*Tertulliani*  
79 and *Maramai*, 1998; *Rovida et al.*, 2016; *Bonini et al.*, 2016) and the most recent  $M_w$  5.1 earthquake  
80 in 2013 (*Pezzo et al.*, 2014; *Stramondo et al.*, 2014; *Molli et al.*, 2016).

81 The uppermost stratigraphy at Prà di Lama consists of ~~an~~ 8m-thick layer of alluvial and  
82 palustrine gravels and sandy deposits containing ~~peaty~~ levels, covering an ~85m-thick sandy-to-silty  
83 fluvio-lacustrine deposits with low permeability (from Villafranchian to present age) (*Chetoni*, 1995)  
84 (Fig.2a and b). These deposits cover a ~1000m-thick turbiditic sequence (Macigno Fm). Below it, a  
85 sequence of carbonate rocks pertaining to the Tuscan Nappe Unit is present reaching down to a  
86 depth of ~2000 m, where anhydrites (Burano fm.) and calcareous-dolomitic breccias (Calcare  
87 Cavernoso Fm.) overlie the Tuscan Metamorphic Units (Fig. 2c).

88 The Prà di Lama lake lies at the centre of a depression (Figs. 2 and 5). The low slopes  
89 characterizing the topography of the area results in the absence of active gravitational ground  
90 motions (Fig 2). Furthermore, the Prà di Lama sinkhole is an isolated feature in the region being the  
91 only mapped sinkhole in the entire Garfagnana graben (*Caramanna et al.*, 2008); the closest  
92 sinkhole is in Camaiore (*Buchignani et al.*, 2008) near the Tuscany coast (Fig.1).

93 The Prà di Lama sinkhole is located at the intersection between two seismically active faults:  
94 the Corfino normal fault (*Itacha working group, 2003*; *Di Naccio et al.*, 2013; *Itacha working group,*  
95 ~~2003~~-*ISIDe working group*, 2016) and the right-lateral strike-slip fault M.Perpoli-T.Scoltenna that  
96 recently generated the  $M_w$  4.8 earthquake in January 2013 (Fig.1) (*Vannoli*, 2013; *Pinelli*, 2013;  
97 *Molli et al.*, 2017). Hot water springs are also present at Prà di Lama (*Bencini et al.*, 1977; *Gherardi*  
98 and *Pierotti*, 2018). Geochemical analyses of the Prà di Lama spring waters by *Gherardi and Pierotti*

99 (2018), expanding on previous research (*Baldacci et al., 2007*), suggest that both shallow and deep  
100 aquifers are present below Prà di Lama (Fig. 2b). Shallow aquifers have low salinity and low  
101 temperature while waters feeding the thermal springs have high temperature (~57 °C) and high  
102 salinity (5.9g/kgw), suggesting the presence of a deep aquifer at ~2000 m into the anhydrite and the  
103 calcareous-dolomitic breccia. The high salinity of the deep groundwaters is associated with  
104 dissolution of the deep evaporitic formations. Furthermore, un-mixing of deep and shallow waters  
105 is interpreted by *Gherardi and Pierotti (2018)* as an evidence of their rapid upwelling, likely occurring  
106 along the existing faults.

107 **3. Data**

108 Century-scale historical records of sinkhole activity are available at Prà di Lama and allow us  
109 to determine the timescale of sinkhole evolution as well as to characterize the different events of  
110 unrest, in particular the two most recent events in 1996 and 2016. InSAR time-series analysis is also  
111 carried out to measure ground deformations in the Prà di Lama sinkhole in the time period between  
112 events of unrest. Finally, the local catalogue of seismicity (ISIDE catalogue, INGV) is used to inform  
113 us on the timing and types of brittle failures in the area of the sinkhole.

114 **3.1 Historical Record**

115 The first historical record of the Prà di Lama sinkhole dates back to the 991 A.D., when the  
116 area was described as a seasonal shallow pool fed by springs. Since then, the depression grew and  
117 several events of unrest consisting of fracturing and fluctuations of the lake level were reported  
118 (*Raffaelli, 1869; De Stefani, 1879, Giovannetti, 1975*) (Table 1). In particular, eight events of unrest  
119 were reported, giving an average of 1 event of unrest every 26 years. We conducted direct  
120 observation of surface deformation around the lake for the two most recent events in 1996 and  
121 2016.

122 In 1996, the lake level experienced a fall of up to 4 m (Fig. 3 and Fig. S1) and at the same time  
123 the springs outside the lake suddenly increased~~d~~ the water outflow. Clay and mud were also ejected  
124 by the springs outside the lake while fractures and slumps occurred within the lake due to the water  
125 drop (Fig. 3 and Fig. S1). The unrest lasted approximately 2 months, from March to April 1996.  
126 During the final stages, the water level in the lake rose rapidly~~z~~, recovering its initial level~~z~~ and  
127 contemporaneously the springs water flow reduced.

128 In June 2016, an event of unrest consisting of ground subsidence on the western and southern sides  
129 of the Prà di Lama lake started and lasted approximately 9 months, until February 2017. During this  
130 period fractures formed and progressively grew, increasing their throw to up to 70 cm and affecting  
131 a large area on the western side of the lake (Fig. 3 and Fig. S2). Subsidence around the lake resulted  
132 in an increase of the lake surface~~z~~, in particular on the western side and in the formation of tensile  
133 fractures (Fig. 3 and Fig. S2). Unlike the 1996 events of unrest, no lake level changes or increase of  
134 water flow from the springs around the lake were observed.

### 135 3.2 InSAR

136 InSAR is ideally suited to monitor localized ground deformation such as caused by sinkholes  
137 as it can observe rapidly evolving deformation of the ground at high spatial resolution (*Baer et al.*,  
138 *2002; Castañeda et al., 2009; Atzori et al., 2015; Abelson et al., 2017*). Furthermore, the availability  
139 of relatively long datasets of SAR images in the Apennine allows us to study the behaviour of the  
140 Prà di Lama sinkhole using multi-temporal techniques. We processed a total of 200 interferograms  
141 using SAR images acquired by the ENVISAT satellite between 2003 to 2010 from two distinct tracks  
142 in Ascending or Descending viewing geometry (tracks 215 and 437). We used the Small BAseLine  
143 Subset (SBAS) multi-interferogram method originally developed by *Berardino et al. (2002)* and  
144 recently implemented for parallel computing processing (P-SBAS) by *Casu et al. (2014)* to obtain  
145 incremental and cumulative time-series of InSAR Line-of-Sight (LOS) displacements as well as maps

146 of average LOS velocity. In particular, the InSAR processing has been carried out via the ESA platform  
147 P-SBAS open-access on-line tool named G-POD (Grid Processing On Demand) that allows generating  
148 ground displacement time series from a set of SAR data (*De Luca et al., 2015*).

149 The P-SBAS G-POD tool allows the user to set some key parameters to tune the InSAR  
150 processing. In this work, we set a maximum perpendicular baseline (spatial baseline) of 400 m and  
151 maximum temporal baseline of 1500 days. The geocoded pixel dimension was set to ~80 m by 80 m  
152 (corresponding to averaging together 20 pixels in range and 4 pixels in azimuth).

153 We initially set a coherence threshold to 0.8 (0 to 1 for low to high coherence) in order to  
154 select only highly coherent pixels in our interferograms. The 0.8 coherence threshold is used to  
155 select the pixels for the phase unwrapping step that is carried out by the Extended Minimum Cost  
156 Flow (EMCF) algorithm (*Pepe and Lanari, 2006*). By setting high values of this parameter the pixels  
157 in input to the EMCF algorithm are affected by less noise as compared to selecting low values, thus  
158 increasing the quality of the phase unwrapping step itself and reducing the noise in our final velocity  
159 maps and time-series (*De Luca et al., 2015; Cignetti et al., 2016*).

160 We also inspected the series of interferograms and excluded individual interferograms with low  
161 coherence. We identified and discarded 29 noisy interferograms in track 215A and other 11  
162 interferograms in track 437D. Finally, we applied an Atmospheric Phase Screen (APS) filtering to  
163 mitigate further atmospheric disturbances (*Hassen, 2001*). Accordingly, we used a triangular  
164 temporal filter with a width of 400 days to minimize temporal variations shorter than about a year  
165 as we focus on steady deformations rather than seasonal changes. Shorter time interval of 300 days  
166 was also tested but provided more noisy time-series.

167 The average velocity map and the incremental time-series of deformation obtained with the  
168 P-SBAS method have to be referred to a stable Reference Point. For our analysis, the reference point  
169 was initially set in the city of Massa because GPS measurements from *Bennett et al. (2012)* show

170 that the surface velocities there are < 1mm yr<sup>-1</sup>; therefore, Massa can be considered stable.  
171 Assuming Massa as reference point, the average velocity map revealed the deformation pattern  
172 around the Prà di Lama lake. We then moved the reference point outside the sinkhole deformation  
173 pattern but close to the village of Pieve Fosciana town (Fig. S3a). Selecting a reference point close  
174 to our study area rather than in Massa allowed us to better minimize the spatially correlated  
175 atmospheric artefacts.

176 As a final post processing step we also calculated the vertical and east-west components of the  
177 velocity field in the area covered by both the ascending and descending tracks and assuming no  
178 north-south displacement. Given that the study area is imaged by the ENVISAT satellite from two  
179 symmetrical geometries with similar incidence angles (few degrees of difference), the vertical and  
180 east-west components of the velocity field can simply be obtained solving the following system of  
181 equations (*Manzo et al., 2006*):

$$182 \begin{cases} v_H = \frac{\cos \vartheta}{\sin(2\vartheta)} (v_{DESC} - v_{ASC}) = \frac{v_{DESC} - v_{ASC}}{2 \sin \vartheta} \\ v_V = \frac{\sin \vartheta}{\sin(2\vartheta)} (v_{DESC} + v_{ASC}) = \frac{v_{DESC} + v_{ASC}}{2 \cos \vartheta} \end{cases}$$

183 where  $v_H$  and  $v_V$  are the horizontal and vertical component of the velocity field,  $v_{DESC}$  and  $v_{ASC}$   
184 are the average LOS velocities in the Descending and Ascending tracks, respectively;  $\vartheta$  is the  
185 incidence angle.

186 The InSAR P-SBAS analysis shows that significant surface deformation occurs at Pieve Fosciana  
187 between 2003 and 2010. The observed deformation pattern consists of range increase mainly on  
188 the western flank of the Prà di Lama lake. The range increase is observed in both ascending and  
189 descending velocity maps (Fig. 4a, b), with average LOS velocities of up to -7.1 mm  $\text{yr}^{-1}$  decaying to  
190 -1 mm  $\text{yr}^{-1}$  over a distance of 400 m away from the lake. Elsewhere around the lake coherence is not  
191 kept due to the presence of both cropland and woodland cover, leading to decorrelation. However,  
192 few coherent pixels are identified on the eastern flank of the lake, in areas with buildings and sparse

193 vegetation cover, suggesting that the deformation pattern may be circular, with a radius of ~600 m  
194 (Figs. 4 and 5). In order to increase the number of analysed pixels we tested decreasing our  
195 coherence threshold from 0.8 to 0.4. The results are displayed in Fig. S3b and show that only a few  
196 more pixels are gained north of the sinkhole as compared to choosing a threshold of 0.8 (Fig. 4). We  
197 conclude that decreasing the coherence threshold does not allow to retrieve the entire deformation  
198 pattern, likely due to the fact the area is vegetated.

199 The maps of vertical and East-West velocities show vertical rates of  $-4.6 \text{ mm yr}^{-1}$  and horizontal  
200 eastward velocities of  $5.4 \text{ mm yr}^{-1}$  (Fig. 4c, d) consistent with subsidence and contraction centred at  
201 the lake. Furthermore, figure 5 shows that the current deformation pattern follows the topography,  
202 suggesting that subsidence at Prà di Lama is a long-term feature. The time-series of cumulative LOS  
203 displacements show that subsidence occurred at an approximately constant rate between the 2003  
204 and the 2008 but it slowed down in 2008 (Fig. 4e, f), indicating that subsidence at Prà di Lama occurs  
205 also between events of unrest. Furthermore, our time-series of vertical and east-west cumulative  
206 displacements also confirm that the fastest subsidence and contemporaneous eastward motion  
207 occurred until 2008 (Fig. 4 g, h). In order to better understand the mechanisms responsible for the  
208 sinkhole growth and the different types of episodic unrest we also analysed the seismicity.

### 209 **3.3 Seismicity**

210 ~~We analysed the S~~ seismicity at the Prà di Lama lake was analysed using the catalogue ISIDE  
211 (Italian Seismological Instrumental and Parametric Data-Base) spanning the time period from 1986  
212 to 2016. We calculated the cumulative seismic moment release using the relation between seismic  
213 moment and magnitudes given by *Kanamori* (1977). First, we analysed the seismic moment release  
214 and the magnitude content of the earthquakes in the area encompassing the sinkhole and the faults  
215 intersection (10 km radius, Fig. 1) to understand whether unrest at Prà di Lama is triggered by  
216 earthquakes along the active faults (Fig. 6). Figure 6a shows that although several seismic swarms

217 occurred in the area, no clear temporal correlation between the swarms and the events of unrest  
218 at Prà di Lama is observed, suggesting that the majority of seismic strain released on faults around  
219 the Prà di Lama lake does not affect the activity of the sinkhole. We removed from the plot in  
220 figure[Fig. 6a](#) the large magnitude earthquake,  $M_w$  4.8, on the 25<sup>th</sup> of January, 2013 in order to better  
221 visualize the pattern of seismic moment release in time. In any case, no activity at Prà di Lama was  
222 reported in January 2013.

223 We also analysed the local seismicity around the Prà di lama lake, within a circular area of 3  
224 km radius around the lake (Fig. 1), to better understand the deformation processes occurring at the  
225 sinkhole and we found that swarms of small-magnitude earthquakes ( $M_L \leq 2$ ) occurred during both  
226 events of unrest at Prà di Lama in 1996 and 2016 (Fig. 7a, b, c), while a few earthquakes with  
227 magnitudes  $> 2$  occurred irrespective of the events of unrest. This indicates that seismicity during  
228 sinkhole activity is characterized by seismic energy released preferentially towards the small end of  
229 magnitudes spectrum. This pattern is specific of the sinkhole area as in the broader region (Fig. 6b,  
230 c) the majority of earthquakes magnitudes are in the range between  $M_L > 2$  and  $M_L < 3$  and few  $M_L$   
231  $> 3$  also occurred. We also analysed the hypocentres of the earthquakes around the Prà di lama lake  
232 (3 km radius) and find that these range between 4.5 and 11.5 km depth, indicating that deformation  
233 processes in the fault zone control the sinkhole activity. On the other hand, no earthquakes were  
234 recorded at Prà di Lama during the period of subsidence identified by InSAR between 2003 and  
235 2010, indicating that subsidence between events of unrest continues largely aseismically.

236 To strengthen our seismicity analysis and clarify whether a connection between major  
237 tectonic earthquakes and sinkhole unrest exists, we also analysed the historical parametric seismic  
238 catalogues (Rovida *et al.*, 2016; INGV Catalogo Parametrico dei Terremoti Italiani, CPTI15). Figure 8  
239 shows the occurrence of major earthquakes, with magnitude  $> 4.0$  up to 20 km distant from Pieve  
240 Fosciana and the events of sinkhole unrest at Prà di lama. No clear connection between occurrence

241 of large distant earthquakes and events of sinkhole unrest is observed, suggesting that the  
242 mechanisms responsible for activation of the Prà di Lama sinkhole should be attributed to local  
243 processes.

244 **4. Discussion and conclusions**

245 A multi-disciplinary dataset of InSAR measurements, field observations and seismicity reveal  
246 that diverse deformation events occur at the Prà di Lama sinkhole. Two main events of sinkhole  
247 unrest occurred at Prà di Lama in 1996 and 2016 but the processes had different features. In 1996  
248 the lake-level dropped together with increased water outflow from the springs, while in 2016  
249 ground subsidence led to the expansion of the lake surface and fracturing. In 2016, fractures form ed  
250 on the South-Western shore of the lake. The main active strike-slip fault is also oriented SW,  
251 suggesting a possible tectonic control on the deformation.

252 We ~~also~~ considered processes not related to the sinkhole activity that could explain the  
253 observed deformation at Prà di Lama. Active landslides can cause both vertical and horizontal  
254 surface motions (e.g. *Nishiguchi et al., 2017*). However, no landslides are identified in the deforming  
255 area around the sinkhole (Fig.3). Furthermore, the low topographic slopes rule out the presence of  
256 active landslides in the area. Concentric deformation patterns are observed above shallow aquifers  
257 (e.g. *Amelung et al., 1999*). However, deformation caused by aquifers have a seasonal pattern rather  
258 than continuous subsidence over the timespan of several years, as in Prà di Lama. A long-term  
259 subsidence could only be caused by over-exploitation of an aquifer but no water is pumped from  
260 the aquifers in the deforming area around Prà di Lama. We conclude that the observed InSAR  
261 deformation is caused by the sinkhole.

262 InSAR analysis shows that continuous but aseismic subsidence of the sinkhole occurred  
263 between the two events of unrest, during the period 2003-2010. Instead swarms of small-  
264 magnitude earthquakes coeval to the unrest events of 1996 and 2016 were recorded at depth

265 between 4.5 and 11.5 km, indicating that a link between low magnitude seismicity and sinkhole  
266 activity exists. We suggest that seismic creep in the fault zone underneath Prà di Lama occurs,  
267 causing the diverse deformation events.

268 Seismic creep at depth could have induced pressure changes in the aquifer above the fault  
269 zone (1996 events) as well as causing subsidence by increased fracturing (2016 events). The  
270 seismicity pattern revealed by our analysis suggests that the Mt.Perpoli-T.Scoltenna strike-slip fault  
271 system underneath Prà di Lama is locally creeping, producing seismic sequences of low magnitude  
272 earthquakes. Similar seismicity patterns were observed along different active faults (*i.e.* [Nadeau et al., 1995](#);  
273 [Linde et al. 1996](#); [Nadeau et al., 1995](#); [Rau et al., 2007](#); [Chen et al., 2008](#); [Harris, 2017](#)). In  
274 2006, along the Superstition Hills fault (San Andreas fault system, California) seismic creep has been  
275 favoured by high water pressure ([Scholz, 1998](#); [Wei et al., 2009](#); [Scholz, 1998](#); [Harris, 2017](#)). We  
276 suggest that along the fault zone below Prà di Lama an increase in pressure in the aquifer in 1996  
277 caused fracturing at the bottom of the lake and upward migration of fluids rich in clays, in agreement  
278 with the observations of lake-level drop and mud-rich water ejected by the springs in 1996. Our  
279 interpretation is also in agreement with geochemical data indicating that the high salinity of thermal  
280 waters at Prà di Lama have a deep origin, ~2000 m, where fluid circulation dissolves evaporites and  
281 carbonates, creating cavities and then reaching the surface by rapid upwelling along the faults  
282 system ([Gherardi and Pierotti, 2018](#)). The presence of deep cavities and a thick non-carbonate  
283 sequence suggests that the Prà di Lama sinkhole is a deep-sited caprock collapse sinkhole according  
284 to the sinkhole classification of [Gutiérrez et al. \(2008, 2014\)](#). Sudden fracturing and periods of  
285 compaction of cavities created by enhanced rock dissolution and upward erosion in the fluid  
286 circulation zone could explain both sudden subsidence and fracturing, as in 2016, and periods of  
287 continuous but aseismic subsidence as in 2003-2010. Similar processes have been envisaged for the  
288 formation of a sinkhole at the Napoleonville Salt Dome, where a seismicity study suggests that

289 fracturing enhanced the rock permeability, promoting the rising of fluids and, as a consequence,  
290 erosion and creation of deep cavities prone to collapse (*Sibson, 1996; Micklethwaite et al., 2010;*  
291 *Nayak and Dreger, 2014; Yarushina et al., 2017; Sibson, 1996; Micklethwaite et al., 2010, Nayak and*  
292 *Dreger, 2014*). Recently, a sequence of seismic events was identified at Mineral Beach (Dead Sea  
293 fault zone) and was interpreted as the result of cracks formation and faulting above subsurface  
294 cavities (*Abelson et al., 2017*).

295 Precursory subsidence of years to few months has been observed to precede sinkhole collapse  
296 in carbonate or evaporitic bedrocks (e.g. *Baer et al., 2002; Nof et al., 2013; Cathleen and Bloom,*  
297 *2014; Atzori et al., 2015; Abelson et al., 2017*). However, the timing of these processes strongly  
298 depends on the rheological properties of the rocks (*Shalev and Lyakhovsky, 2013*). Furthermore, the  
299 presence of a thick lithoid sequence in Prà di Lama may delay sinkhole collapse, also in agreement  
300 with the exceptionally long timescale (~200 years) of growth of the Prà di Lama sinkhole (*-Shalev*  
301 *and Lykovsky, 2012; Abelson et al., 2017*). However, at present we are not able to establish if and  
302 when a major collapse will occur in Prà di Lama.

303 We identified a wide range of surface deformation patterns associated with the Prà di Lama  
304 sinkhole and we suggest that a source mechanism for the sinkhole formation and growth is seismic  
305 creep in the active fault zone underneath the sinkhole. This mechanism could control the evolution  
306 of other active sinkholes in Italy as well as in other areas worldwide where sinkhole form in active  
307 fault systems (e.g. Dead Sea area). InSAR monitoring has already shown to be a valid method to  
308 detect precursory subsidence occurring before a sinkhole collapse and the recent SAR missions, such  
309 as the European Sentinel-1, will very likely provide a powerful tool to identify such deformations.

310  
311  
312  
313  
314

315 **References**

316 Abelson, M., Aksinenko, T., Kurzon, I., Pinsky, V., Baer, G., Nof, R., & Yechieli, Y.: Nanoseismicity forecast  
317 sinkhole collapse in the Dead Sea coast years in advance. <https://doi.org/10.1130/G39579.1>, 2017

318 Amelung, F., Galloway, D.L., Bell, J.W., Zebker, H.A., and Lacznak, R.J.: Sensing the ups and downs of Las  
319 Vegas: InSAR reveals structural control of land subsidence and aquifer-system deformation. *Geology*,  
320 27 (6), 483-486. [https://doi.org/10.1130/0091-7613\(1999\)027<0483:STUADO>2.3.CO;2](https://doi.org/10.1130/0091-7613(1999)027<0483:STUADO>2.3.CO;2), 1999

321 Atzori, S., Baer, G., Antonioli, A., & Salvi, S.: InSAR-based modelling and analysis of sinkholes along the Dead  
322 Sea coastline. *Geophysical Research Letters*, 42, 8383–8390. <https://doi.org/10.1002/2015GL066053>,  
323 2015

324 Baldacci, F., Botti, F., Cioni, R., Molli, G., Pierotti, L., Scorzari, A., Vaselli, L.: Geological-structural and  
325 hydrogeochemical studies to identify seismically active structures: case history from the Equi Terme-  
326 Monzone hydrothermal system (Northern Apennine – Italy). *Geoitalia, 6th Italian Forum of Earth  
327 Sciences. Rimini*, 2007

328 Bencini, A., Duchi, V., Martini, M.: Geochemistry of thermal springs of Tuscany (Italy). *Chemical Geology*, 19,  
329 229-252, 1977

330 Baer, G., Schattner, U., Wachs D., Sandwell, D., Wdowinski, S., Frydman, S.: The lowest place on Earth is  
331 subsiding – An InSAR (Interferometric Synthetic Aperture Radar) Perspective. *Geological Society of  
332 America Bulletin*, 114 (1), 12-23. [https://doi.org/10.1130/00167606\(2002\)114<0012:TLPOEI>2.0.CO;2](https://doi.org/10.1130/00167606(2002)114<0012:TLPOEI>2.0.CO;2),  
333 2002

334 Bennet, R.A., Serpelloni, E., Hreinsdottir, S., Brandon, M.T., Buble, G., Basic T., Casale, G., Cavaliere, A.,  
335 Anzidei, M., Marjonovic, Minelli, G., Molli, G., & Montanari, A.: Syn-convergent extension observed  
336 using the RETREAT GPS network, northern Apennines, Italy. *Journal of Geophysical Research*, 117.  
337 <https://doi.org/10.1029/2011JB008744>, 2012

338 Berardino, P., Fornaro, G., Lanari, R., & Sansosti, E.: A new algorithm for surface deformation monitoring  
339 based on Small Baseline Differential SAR interferograms. *IEEE International Geoscience and Remote  
340 Sensing Symposium*, 40(11). <https://doi.org/10.1109/TGRS.2002.803792>, 2002

341 Bonini, M., Corti, G., Donne, D. D., Sani, F., Piccardi, L., Vannucci, G., Genco, R., Martelli, L., Ripepe, M.: Seismic  
342 sources and stress transfer interaction among axial normal faults and external thrust fronts in the  
343 northern Apennines (Italy): a working hypothesis based on the 1916-1920 time-space cluster of  
344 earthquakes. *Tectonophysics*, 680, 67–89. <https://doi.org/10.1016/j.tecto.2016.04.045>, 2016

345 **Buchignani, V., D'Amato Avanzi, G., Giannecchini, R., Puccinelli, A.: Evaporite karst and sinkholes: a synthesis  
346 on the case of Camaiore (Italy). *Environmental Geology*, 53, 1037-  
347 1044. <https://doi.org/10.1007/s00254-007-0730-x>, 2008**

348 Caramanna, G., Ciotoli, G., Nisio, S.: A review of natural sinkhole phenomena in Italian plain areas. *Natural  
349 Hazards*, 45, 145–172. <https://doi.org/10.1007/s11069-007-9165-7>, 2008

350 Castañeda, C., Gutiérrez, F., Manunta, M., Galve, J. P.: DInSAR measurements of ground deformation by  
351 sinkholes, mining subsidence, and landslides, Ebro River, Spain. *Earth Surf. Process. Landforms*, 34, 11,  
352 1562–1574. <https://doi.org/10.1002/esp.1848>, 2009

353 Casu, F., Elefante, S., Imperatore, P., Zinno, I., Manunta, M., De Luca, C., & Lanari, R: SBAS-DInSAR parallel  
354 processing for deformation time-series computation. *IEEE Journal of Selected Topics in Applied Earth*  
355 *Observations and Remote Sensing*, 7(8), 3285–3296. <https://doi.org/10.1109/JSTARS.2014.2322671b>,  
356 2014

357 Cathleen, J., & Blom, R.: Bayou Corne, Louisiana, sinkhole: Precursory deformation measured by radar  
358 interferometry. *Geology*. 42 (2), 111-114. <https://doi.org/10.1130/G34972.1>, 2014

359 Chen, K.H., Nadeau, R.M., Rau, R.: Characteristic repeating earthquakes in an arc-continent collision  
360 boundary zone: The Chihshang fault of eastern Taiwan. *Earth and Planetary Science Letters*.  
361 <https://doi.org/10.1016/j.epsl.2008.09.021>, 2008

362 Chetoni, R.: Terme di Prà di Lama (Pieve Fosciana, Lu), indagine geognostica sulle aree dissestate nel marzo  
363 1996. *Geological Report*, 1996

364 Cignetti, M., Manconi, A., Manunta, M., Giordan, D., De Luca, C., Allasia, P., Ardizzone, F.: Taking Advantage  
365 of the ESA G-POD Service to Study Ground Deformation Processes in High Mountain Areas: A Valle  
366 d'Aosta Case Study, Northern Italy. *Remote Sensing*, 8, 852. <https://doi.org/10.3390/rs8100852>, 2016

367 Closson, D.: Structural control of sinkholes and subsidence hazards along the Jordanian Dead Sea coast.  
368 *Environmental Geology*, 47 (2), 290-301. <https://doi.org/10.1007/s00254-004-1155-4>, 2005

369 Closson, D., Karaki, N.A., Klinger, Y., & Hussein, M. J.: Subsidence and Sinkhole Hazard Assessment in the  
370 Southern Dead Sea Area, Jordan. *Pure and Applied Geophysics*, 162, 221–248.  
371 <https://doi.org/10.1007/s00024-004-2598-y>, 2005

372 Rovida A., Locati M., Camassi R., Lolli B., Gasperini P.: CPTI15, the 2015 version of the Parametric Catalogue  
373 of Italian Earthquakes. Istituto Nazionale di Geofisica e Vulcanologia. <http://doi.org/10.6092/INGV.IT-CPTI15>, 2016

375 De Luca, C., Cuccu, R., Elefante, S., Zinno, I., Manunta, M., Casola, V., Rivolta, G., Lanari, R., Casu, F.: An On-  
376 Demand Web Tool for the Unsupervised Retrieval of Earth's Surface Deformation from SAR Data: The  
377 P-SBAS Service within the ESA G-POD Environment. *Remote Sensing*, 7(11), 15630-15650.  
378 <https://doi.org/10.3390/rs71115630>, 2015

379 De Stefani, C.: Le Acque Termali di Pieve Fosciana. *Memorie della Società Toscana di Scienze Naturali*, 4, 72-  
380 97, 1879

381 Del Prete, S., Iovine, G., Parise, M., Santo, A.: Origin and distribution of different types of sinkholes in the  
382 plain areas of Southern Italy. *Geodinamica Acta* 23/1-3, 113-127. <https://doi.org/10.3166/ga.23.113-127>, 2010

384 Di Naccio, D., Boncio, P., Brozzetti, F., Pazzaglia, F. J., & Lavecchia, G.: Morphotectonic analysis of the  
385 Lunigiana and Garfagnana grabens (northern Apennines, Italy): Implications for active normal faulting.  
386 *Geomorphology*, 201, 293–311. <https://doi.org/10.1016/j.geomorph.2013.07.003>, 2013

387 Doglioni, C.: A proposal for the kinematic modelling of the W-dipping subduction – possible applications to  
388 the Tyrrhenian-Apennines system. *Terra Nova*, 3, 423-434. <https://doi.org/10.1111/j.1365-3121.1991.tb00172.x>, 1991

390 Elter, P., Giglia, G., Tongiorgi, M., Trevisan, L.: Tensional and compressional areas in the recent (Tortonian to  
391 Present) evolution of the Northern Apennines. *Bollettino di Geofisica Teorica ed Applicata*, 65 (8), 1975

392 Faccenna, C. Florindo, F., Funiciello, R., Lombardi, S.: Tectonic setting and Sinkhole Features: case histories  
393 from Western Central Italy. *Quaternary Proceedings*, 3, 47–56, 1993

394 Faccenna, C. Becker, T.W., Miller, S.M., Serpelloni, E., & Willet, S.D.: Isostasy, dynamic topography, and the  
395 elevation of the Apennines of Italy. *Earth and Planetary Science Letters*, 407, 163–174.  
396 <https://doi.org/10.1016/j.epsl.2014.09.027>, 1993

397 Florea, L. J.: Using State-wide GIS data to identify the coincidence between sinkholes and geologic structure.  
398 *Journal of Cave and Karst Studies*, (August), 120–124. Retrieved from  
399 [http://digitalcommons.wku.edu/geog\\_fac\\_pub/14](http://digitalcommons.wku.edu/geog_fac_pub/14), 2005

400 Ford, D.C., Williams, P.: Karst Hydrogeology and Geomorphology. *Wiley, Chichester*, (562 pp.), 2007

401 Frumkin, A., & Raz, E.: Collapse and subsidence associated with salt karstification along the Dead Sea.  
402 *Carbonates and Evaporites*, 16(2), 117–130. <https://doi.org/https://doi.org/10.1007/bf03175830>, 2001

403 Giovannetti, F.: Pieve Fosciana Ieri e Oggi. *Amministrazione comunale di Pieve Fosciana, Lucca Province, Italy*  
404 (*51 pp.*), 1975

405 Gherardi, F., Pierotti, L.: The suitability of the Pieve Fosciana hydrothermal system (Italy) as a detection site  
406 for geochemical seismic precursors. *Applied Geochemistry*  
407 <https://doi.org/10.1016/j.apgeochem.2018.03.009>, 2018

408 Gutiérrez, F., Guerrero, J., Lucha, P.: A genetic classification of sinkholes illustrated from evaporite paleokarst  
409 exposures in Spain. *Environmental Geology*, 53. <https://doi.org/10.1007/s00254-007-0727-5>, 2008

410 Gutiérrez, F., Parise, M., De Waele J., Jourde, H.: A review on natural and human-induced geohazards and  
411 impacts in karst. *Earth-Science Reviews*, 138. <https://doi.org/10.1016/j.earscirev.2014.08.002>, 2014

412 Hanssen, R. F.: Radar Interferometry: Data Interpretation and Error Analysis. Kluwer Academic Publisher.  
413 <https://doi.org/10.1007/0-306-47633-9>, 2001

414 Harris, R.A.: Large earthquakes and creeping faults. *Reviews of Geophysics*, 55, 169–198.  
415 <https://doi.org/10.1002/2016RG000539>, 2017

416 Harrison, R. W., Newell, W. L., & Necdet, M.: Karstification Along an Active Fault Zone in Cyprus. Atlanta,  
417 Georgia. *U.S. Geological Survey Water-Resources Investigations Report* 02-4174, 2002

418 ISIDe working group version 1.0, 2016

419 Johnson, A. G., Kovach, R. L., & Nur, A.: Pore pressure changes during creep events on the San Andreas Fault.  
420 *Journal of Geophysical Research*, 78 (5). <https://doi.org/10.1029/JB078i005p00851>, 1973

421 Kanamori, H.: The Energy Release in Great Earthquakes. *Journal of Geophysical Research*, 82(20).  
422 <https://doi.org/10.1029/JB082i020p02981>, 1977

423 Kawashima, K., Aydan, O., Aoki, T., Kishimoto, I., Konagal, K., Matsui, T., Sakuta, J., Takahashi, N., Teodori, S.-  
424 P., Yashima, A.: Reconnaissance investigation on the damage of the 2009 L'Aquila, Central Italy  
425 earthquake. *Journal of Earthquake Engineering* 14, 817–841.  
426 <https://doi.org/10.1080/13632460903584055>, 2010

427 Le Breton, E., Handy, M., Molli, G., & Ustaszewski K.: Post-20 Ma Motion of the Adriatic Plate: New  
428 Constraints from Surrounding Orogenes and Implications for Crust-Mantle Decoupling. *Tectonics*, 36.  
429 <https://doi.org/10.1002/2016TC004443>, 2000

430 Linde, A.T., Gladwin M.T., Johnston, M.J.S., Gwyther, R.L. and Bilham, R.G.: A slow earthquake sequence on  
431 the San Andreas fault. *Nature*, 383. <https://doi.org/10.1038%2F383065a0>, 1996

432 Manzo, M., Ricciardi, G.P., Casu F., Ventura, G., Zeni, G., Borgström S., Berardino, P., Del Gaudio, C., Lanari,  
433 R.: Surface deformation analysis in th Ischia Island (Italy) based on spaceborne radar interferometry.  
434 *Journal of Volcanology and Geothermal Research* 151, 399-416.  
435 <https://doi.org/10.1016/j.jvolgeores.2005.09.010>, 2006

436 Meletti, C., Patacca, E., & Scandone P.: Construction of a Seismotectonic Model: The Case of Italy. *Pure and*  
437 *applied Geophysics*, 157, 11-35. <https://doi.org/10.1007/PL00001089>, 2000

438 Micklethwaite, S., Sheldon, H. A., & Baker, T.: Active fault and shear processes and their implications for  
439 mineral deposit formation and discovery. *Journal of Structural Geology*, 32(2), 151–165.  
440 <https://doi.org/10.1016/j.jsg.2009.10.009>, 2010

441 Molli, G., Torelli, L., & Storti, F.: The 2013 Lunigiana (Central Italy) earthquake: Seismic source analysis from  
442 DInSar and seismological data, and geodynamic implications for the northern Apennines. A discussion.  
443 *Tectonophysics*, 668–669, 108–112. <http://dx.doi.org/10.1016/j.tecto.2015.07.041>, 2016

444

445 Molli, G., Pinelli, G., Bigot, A., Bennett R., Malavieille J., Serpelloni E.: Active Faults in the inner northern  
446 Apennines: a multidisciplinary reappraisal. From 1997 to 2016: Three Destructive Earthquakes along  
447 the Central Apennine Fault system, Italy. July 19<sup>th</sup>-22<sup>nd</sup> 2017 Camerino, Volume Abstract, 2017

448 Nadeau, R.M., Foxal, W., McEvilly, T.V.: Clustering and Periodic Recurrence of Microearthquakes on the San  
449 Andreas Fault at Parkfield, California. *Science*, 267. <https://doi.org/10.1126/science.267.5197.503>,  
450 1995

451 Nayak, A., & Dreger, D. S.: Moment Tensor Inversion of Seismic Events Associated with the Sinkhole at  
452 Napoleonville Salt Dome, Louisiana. *Bullettin of the Seismological Society of America*, 104(4), 1763–  
453 1776. <https://doi.org/10.1785/0120130260>, 2014

454 Neuendorf, K., Mehl, J., Jackson, J.: Glossary of geology, 5th edn. *American Geological Institute*, 779 pp., 2005

455 Nishiguchi, T., Tsuchiya, S., Imaizumi, F.: Detection and accuracy of landslide movement by InSAR analysis  
456 using PALSAR-2 data. *Landslides*, 14:1483–1490. <https://doi.org/10.1007/s10346-017-0821-z>, 2017

457 Nisio, S.: The sinkholes in Tuscany Region. *Memorie Descrittive Carta Geologica d'Italia LXXXV*, 2008

458 Nof, R. N., Baer, G., Ziv, A., Raz, E., Atzori, S., & Salvi, S.: Sinkhole precursors along the Dead Sea, Israel,  
459 revealed by SAR interferometry. *Geology*, 41, (9), 1019-1022. <https://doi.org/10.1130/G34505.1>, 2013

460 Parise, M., Perrone, A., Violante, C., Stewart, J.P., Simonelli, A., Guzzetti, F.: Activity of the Italian National  
461 Research Council in the aftermath of the 6 April 2009 Abruzzo earthquake: the Sinizzo Lake case study.  
462 *Proc. 2nd Int. Workshop “Sinkholes in the Natural and Anthropogenic Environment”, Rome*, pp.  
463 <http://doi.org/623-641.10.13140/2.1.3094.1127>, 2010

464 Parise, M. and Vennari, C.: A chronological catalogue of sinkholes in Italy: the first step toward a real  
465 evaluation of the sinkhole hazard. In: Land L, Doctor DH, Stephenson JB, editors. 2013. *Sinkholes and*

466        *the Engineering and Environmental Impacts of Karst: Proceedings of the Thirteenth Multidisciplinary*  
467        *Conference, May 6-10, Carlsbad, New Mexico: NCKRI Symposium 2. Carlsbad (NM): National Cave and*  
468        *Karst Research Institute.* <http://doi.org/10.5038/9780979542275.1149>, 2013

469        Patacca, E., & Scandone, P.: Post-Tortonian mountain building in the Apennines, the role of the passive  
470        sinking of a relic lithospheric slab. *The Lithosphere in Italy*, 157–176, 1989

471        Pepe, A. and Lanari, R. On the extension of the minimum cost flow algorithm for phase unwrapping of  
472        multitemporal differential SAR interferograms. *IEEE Transaction in Geoscience and Remote Sensing*, 44,  
473        9, 2374–2383. <http://doi.org/10.1109/TGRS.2006.873207>, 2006

474        Pezzo, G., Boncori, J.P.M., Atzori, S., Piccinini, D., Antonioli, A., Salvi, S.: The 2013 Lunigiana (Central Italy)  
475        earthquake: Seismic source analysis from DInSAR and seismological data, and geodynamical implications  
476        for the northern Apennines. *Tectonophysics* 636, 315–324.  
477        <http://dx.doi.org/10.1016/j.tecto.2014.09.005>, 2014

478

479        Pinelli, G.: Tettonica recente e attiva nell'Appennino interno a Nord dell'Arno: una revisione delle strutture e  
480        delle problematiche. Diploma Thesis (89 pp), 2013

481        Raffaelli, R.: Sulle acque termali di Pieve Fosciana, 1869

482        Rau, R., Chen, K.H., Ching, K.: Repeating earthquakes and seismic potential along the northern Longitudinal  
483        Valley fault of Taiwan. *Geophysical Research Letters*, 34. <http://doi.org/10.1029/2007GL031622>, 2007

484        Rovida A., Locati M., Camassi R., Lolli B., Gasperini P.: CPTI15, the 2015 version of the Parametric Catalogue  
485        of Italian Earthquakes. *Istituto Nazionale di Geofisica e Vulcanologia*. <http://doi.org/10.6092/INGV.IT-CPTI15>, 2016

486

487        Salamon, A.: Seismically induced ground effects of the February 11, 2004, M L = 5.2, North-eastern Dead Sea  
488        earthquake. *Geological Survey of Israel Report*, 2004

489        Santo, A., Del Prete, S., Di Crescenzo, G., and Rotella M.: Karst processes and slope instability: some  
490        investigations in the carbonate Apennine of Campania (southern Italy). In: Parise, M., Gunn, J. (Eds.),  
491        *Natural and Anthropogenic Hazards in Karst Areas: Recognition, Analysis, and Mitigation*. *Geological  
492        Society, London*, 279, pp. 59–72. <http://doi.org/10.1144/SP279.60305-8719/07>, 2007

493        Serpelloni, E., Anzidei, M., Baldi, P., Casula, G., & Galvani, A.: Crustal velocity and strain -rate fields in Italy  
494        and surrounding regions: New results from the analysis of permanent and non-permanent GPS  
495        networks. *Geophysical Journal International*, 161(3), 861–880. <https://doi.org/10.1111/j.1365-246X.2005.02618.x>, 2005

496

497        Shalev, E., & Lyakhovsky, V.: Viscoelastic damage modelling of sinkhole formation. *Journal of Structural  
498        Geology*, 42, 163–170. <https://doi.org/10.1016/j.jsg.2012.05.010>, 2012

499        Scholz, C. H.: Earthquakes and friction laws. *Nature*, 391, 37–42. <https://doi.org/10.1038/34097>, 1998

500        Sibson, R. H.: Roughness at the Base of the Seismogenic Zone: Contributing Factors. *Journal of Geophysical  
501        Research*, 87 (B7), 5791-5799. <https://doi.org/10.1029/JB089iB07p05791>, 1984

502        Sibson, R. H.: Structural permeability of fluid-driven fault-fracture meshes. *Journal of Structural Geology*, 18  
503        (8),1031-1042. [https://doi.org/10.1016/0191-8141\(96\)00032-6](https://doi.org/10.1016/0191-8141(96)00032-6), 1996

504 Stramondo, S., Vannoli, P., Cannelli, V., Polcari, M., Melini, D., Samsonov, S., Moro, M., Bignami, C., & Saroli,  
505 M.: X- and C-band SAR surface displacement for the 2013 Lunigiana earthquake (Northern Italy): a  
506 breached relay ramp? *IEEE J. Sel. Top. Appl. Earth Obs. Remote Sens.*  
507 <http://dx.doi.org/10.1109/JSTARS.2014.2313640>, 2014

508 Tertulliani, A., & Maramai, A.: Macroseismic evidence and site effects for the Lunigiana (Italy) 1995  
509 Earthquake. *Journal of Seismology*, 2 (3), 209–222. <https://doi.org/10.1023/A:1009734620985>, 1998

510 Vannoli, P.: Il terremoto in Garfagnana del 25 gennaio 2013 visto dal geologo. Retrieved from  
511 <https://ingvterremoti.wordpress.com/2013/02/06/il-terremoto-del-25-gennaio-2013-visto-dal->  
512 [geologo/#more-3132](#), 2013

513 Wadas, S. H., Tanner, D. C., Polom, U., & Krawczyk, C. M.: Structural analysis of S-wave seismics around an  
514 urban sinkhole; evidence of enhanced suberosion in a strike-slip fault zone. *Natural Hazards and Earth  
515 System Sciences*. <https://doi.org/10.5194/nhess-2017-315>, 2017

516 Wei, M., Sandwell, D., & Fialko, Y.: A silent Mw 4.7 slip event of October 2006 on the Superstition Hills fault,  
517 southern California. *Journal of Geophysical Research*, 114, <https://doi.org/10.1029/2008JB006135>,  
518 2009

519 Yarushina, V. M., Podladchikov, Y.Y., Minakov, A., & Räss, L.: On the Mechanisms of Stress-Triggered Seismic  
520 Events during Fluid Injection. *Sixth Biot Conference on Poromechanics, American Society of Civil  
521 Engineers*. <https://doi.org/10.1061/9780784480779.098>, 2017

522

523

524

525

526

527

528

529

530

531

532

533

534

535

536

537

538

539

540

541

542

543

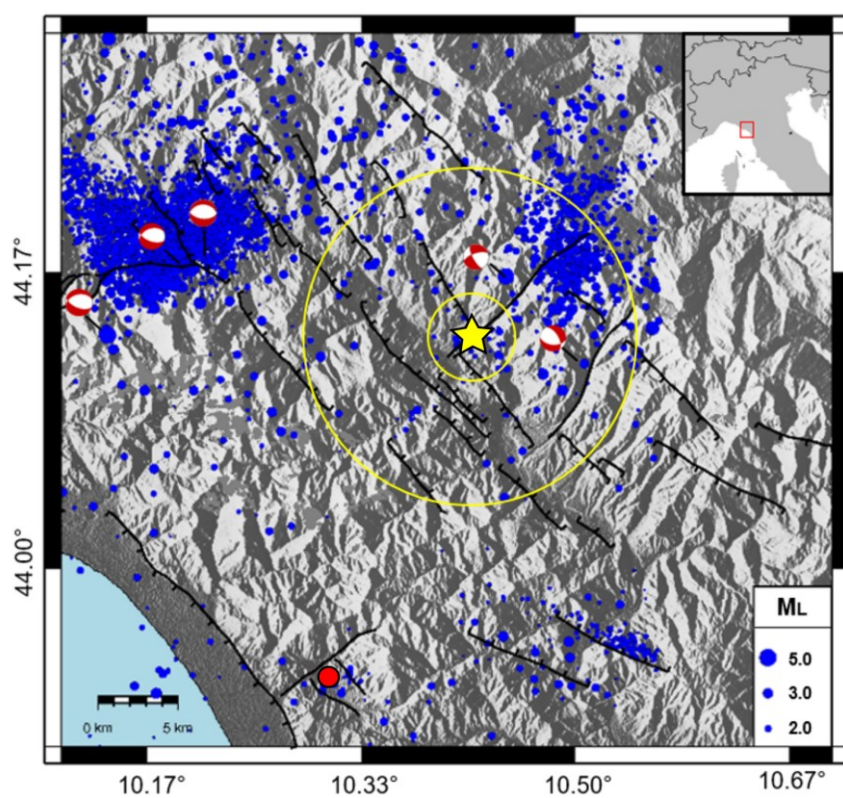
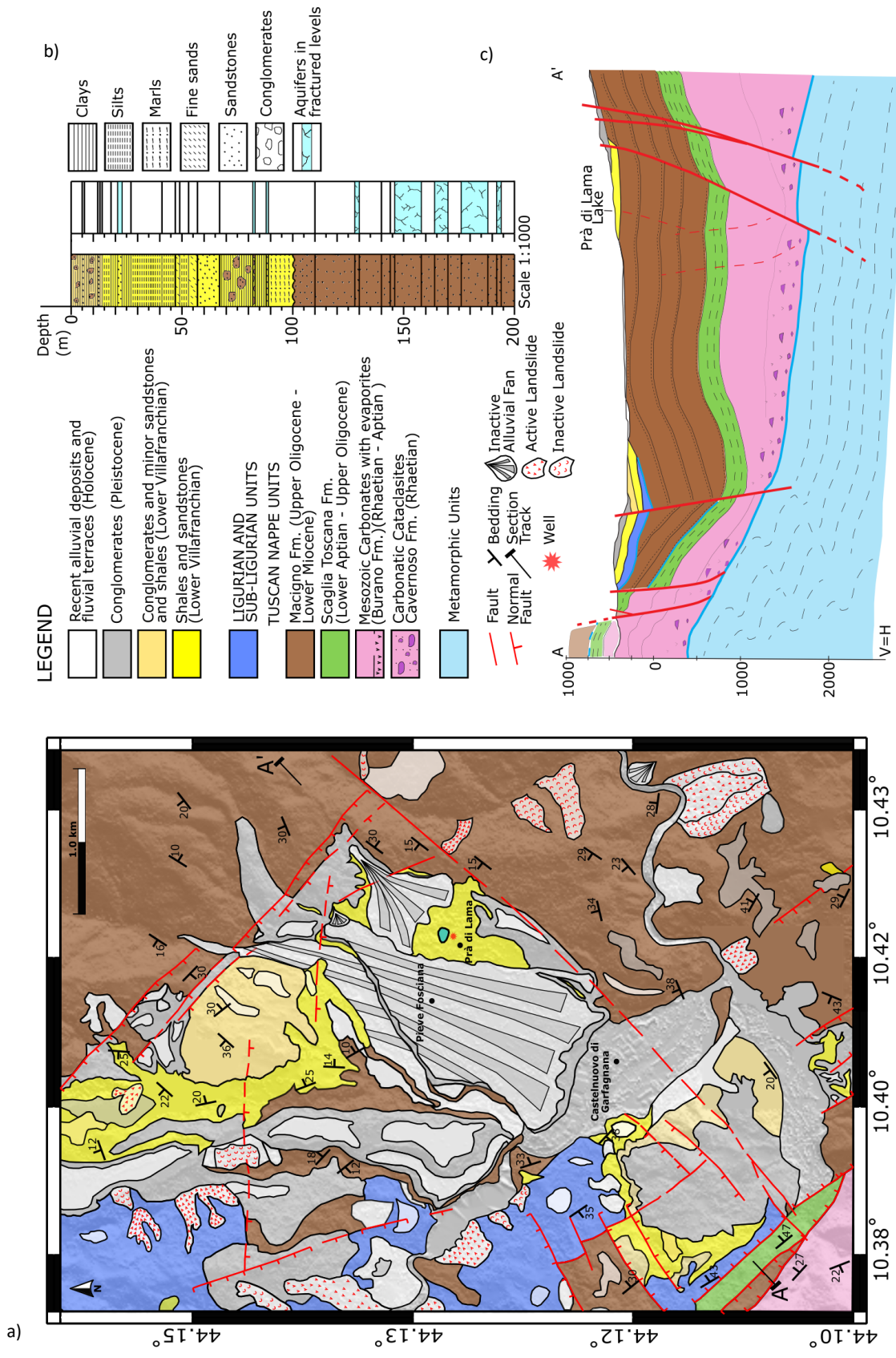


**Figure 1 - Study area.** The Prà di Lama sinkhole is marked by the yellow star. Black tick lines are faults. Blue dots are the earthquakes between 1986 and 2017. Focal mechanisms are from the Regional Centroid Moment Tensor (RCMT) catalogue. The yellow circles represent the areas with radii of 3km and 10 km used for the seismicity analysis. The red dot is the sinkhole of Camaiore ([Buchignani et al., 2008](#); [Caramanna et al. 2008](#)). The red box in the *inset* marks the location of the area shown in the main figure.



563

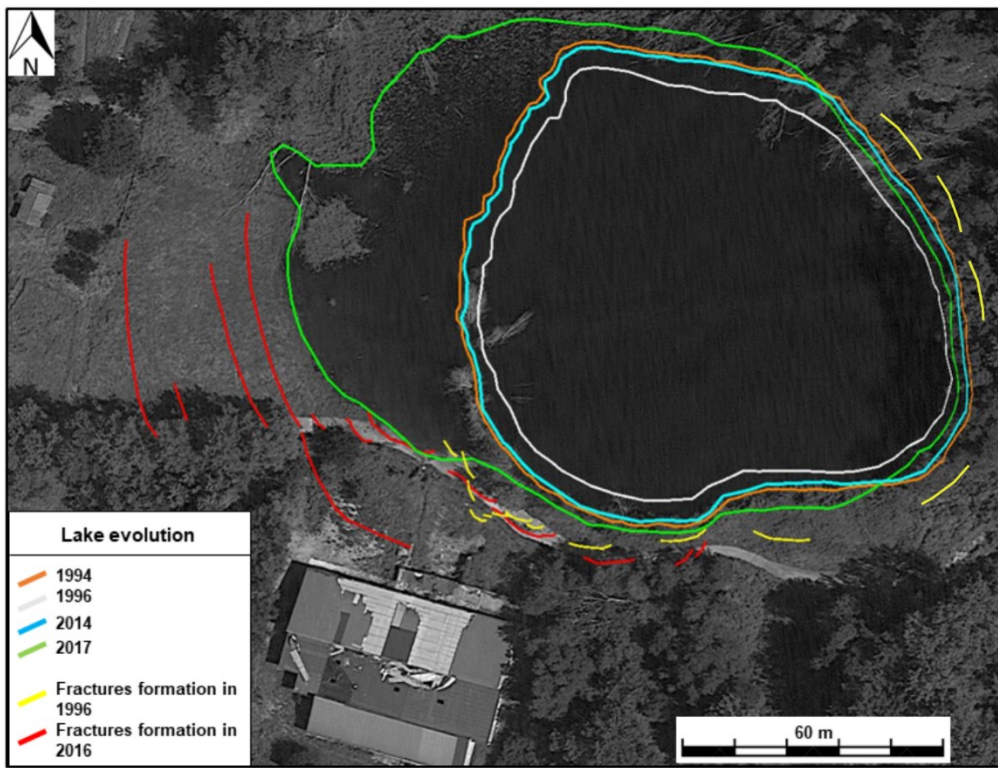
564

565

566

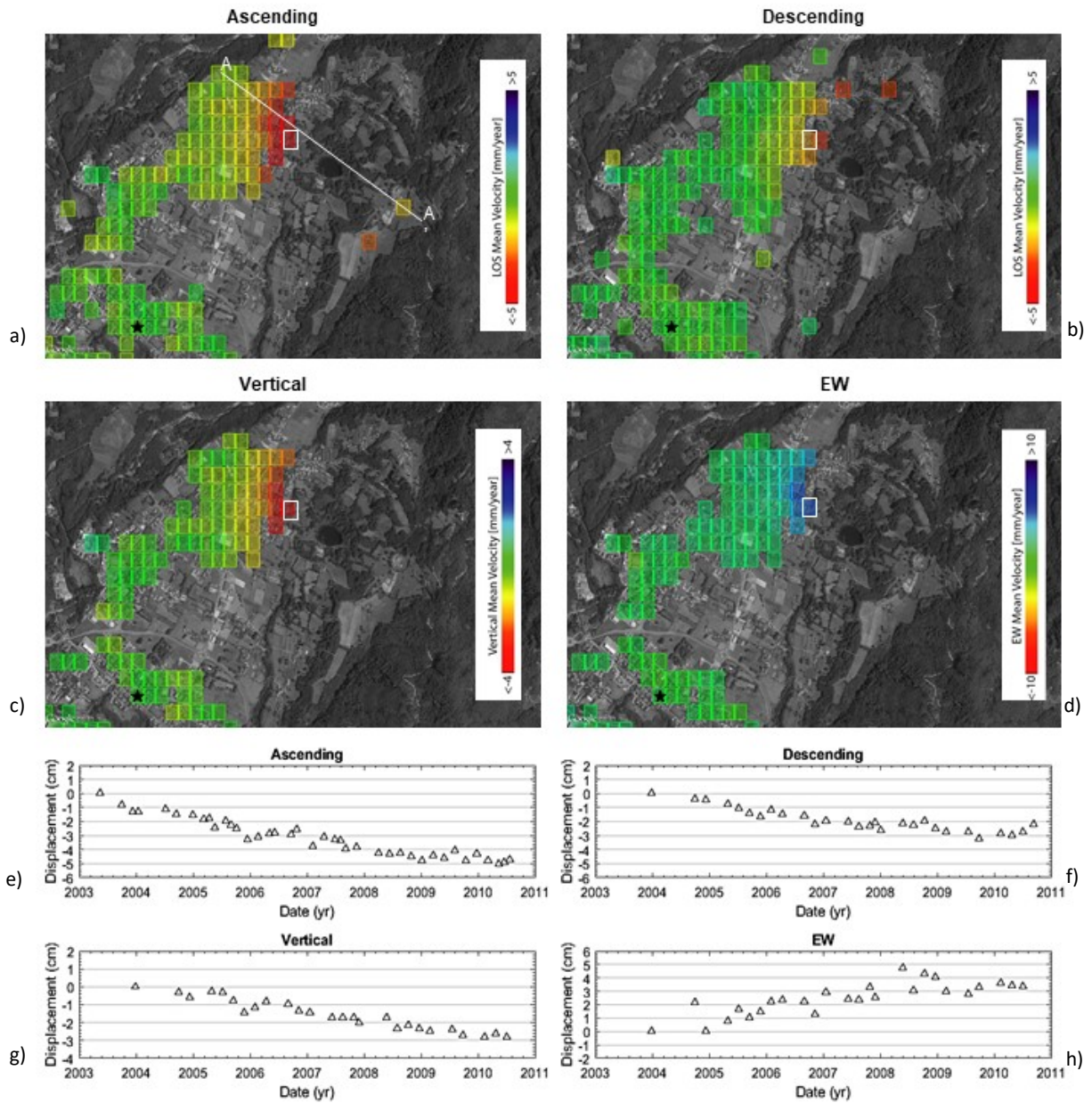
567

**Figure 2 – Geological setting of the study area. a)** Geological, structural and geomorphological map of the area nearby Prà di Lama showing the main tectonic and lithostratigraphic units. **b)** Schematic sedimentary sequence of the Villafranchian deposits obtained from the well drilled at Prà di Lama (Modified from Chetoni 1995). **c)** Stratigraphic cross-section across the Garfagnana graben.



568  
569  
570

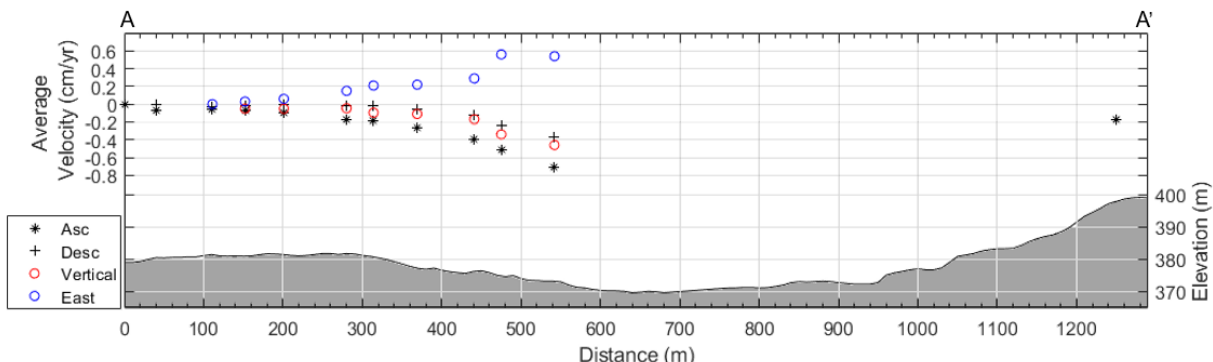
**Figure 3 – Evolution of the Prà di Lama lake between 1994 and 2017.** Lake shores variation have been retrieved from the analysis of Landsat image



571  
572

573 **Figure 4 – a, b)** Maps of average surface velocity and its vertical (c) and East-West (d) components obtained from ENVISAT SAR images  
574 acquired between 2003 and 2010. Negative values indicate range increase. The white line in panel a) marks the cross-section shown  
575 in figure 4. The black star is the point used as reference for the InSAR-SBAS processing. e, f, g, h) Time-series of incremental  
576 deformation extracted from the pixel bounded with the white rectangle.

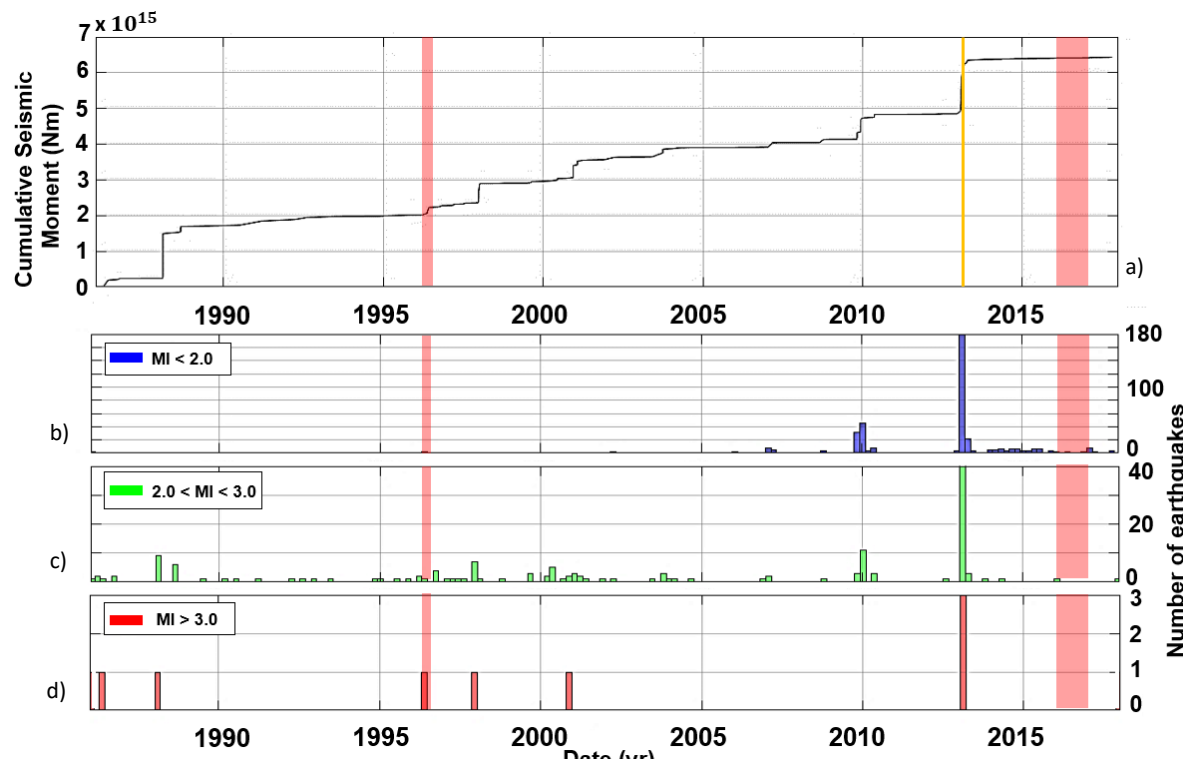
577



578

579 **Figure 5 - Cross-section of topography and InSAR velocities along the A-A' profile as shown in figure 3a.**

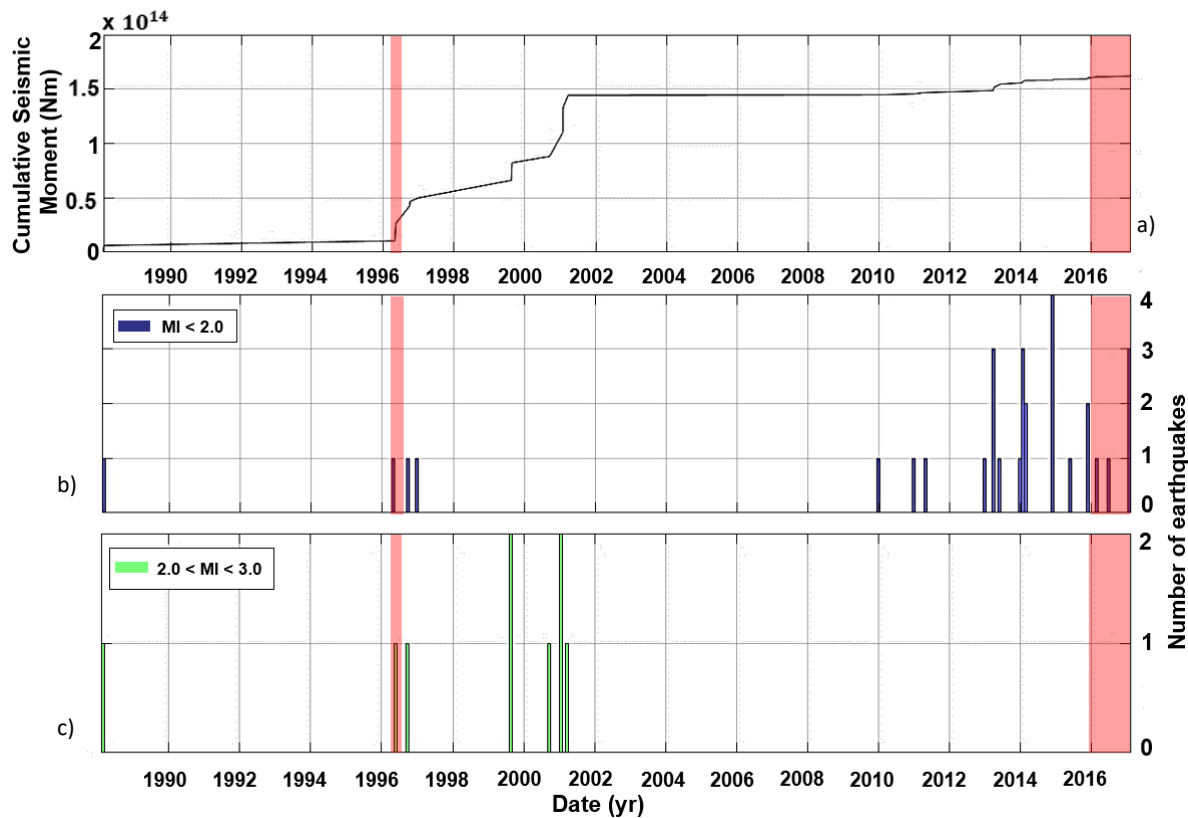
580



581

582 **Figure 6 – Seismicity features of an area 10 km in radius around the Prà di Lama lake.** Cumulative seismic moment released in the  
 583 area (a) and histograms of the number of earthquakes per month. Three different classes of magnitude have been created:  
 584  $MI < 2.0$  (b),  $2.0 < MI < 3.0$  (c) and  $MI > 3.0$  (d). The dataset covers the period between 1986 and 2017. The red transparent bars indicate the  
 585 two events of unrest of 1996 and 2016.

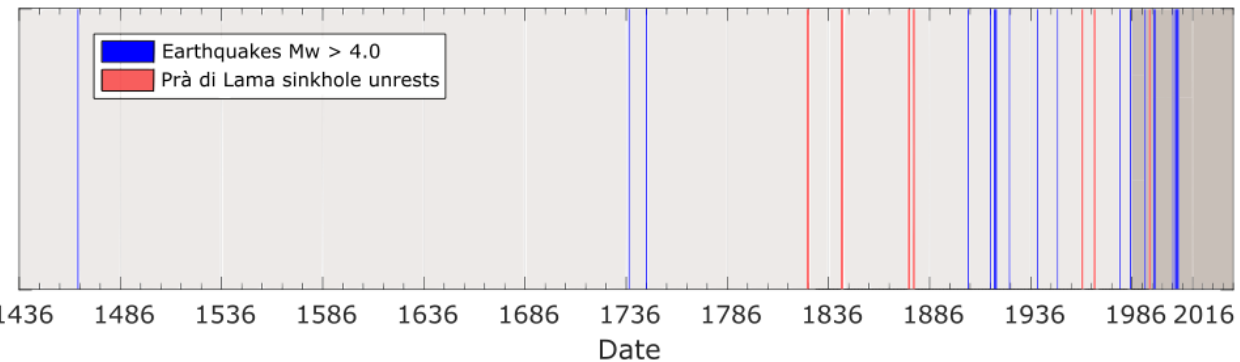
586



587  
588 **Figure 7 - Seismicity features of an area 3 km in radius around the Prà di Lama lake.** Plot of the cumulative seismic moment released  
589 in the area (a) and histograms showing the number of earthquakes occurred each month. Two different classes of Magnitude have  
590 been created: MI < 2.0 (b), 2.0 < MI < 3.0 (c). No events of MI > 3.0 occurred in the area between 1986 and 2017. The red transparent  
591 bars indicate the two events of unrest of 1996 and 2016.

592

593



594 **Figure 8 – Comparison between the earthquakes (blue lines) in the Garfagnana area (INGV Catalogo Parametrico dei Terremoti  
595 Italiani CPTI15, Rovida et al., 2016), and events of unrest at the Prà di Lama sinkhole (red lines).**

596

597

598

599

Year	Brief description of the event
<b>991</b>	Seasonal pool fed by springs
<b>1828</b>	Bursts of the springs water flow. Uprising of muddy waters and clays ( <i>Raffaelli, 1869; De Stefani, 1879</i> )
<b>1843</b>	Bursts of the springs water flow. Uprising of muddy waters and clays ( <i>Raffaelli, 1869; De Stefani, 1879</i> )
<b>1876</b>	Subsidence and fracturing ( <i>De Stefani, 1879</i> )
<b>1877</b>	Subsidence and fracturing ( <i>De Stefani, 1879</i> )
<b>1962</b>	Bursts of the spring water flow. Uprising of muddy waters and clays ( <i>Giovannetti, 1975</i> )
<b>1969</b>	Abrupt falling of the water level and fracturing along the shores. The lake almost disappeared ( <i>Giovannetti, 1975</i> )
<b>1985</b>	Arising of muddy waters in a well
<b>1996</b>	Abrupt fall of the water level and fracturing along the shores
<b>2016-2017</b>	Subsidence and fracturing

601 *Table 1 – Description of the activity at Prà di Lama lake*